AIAA JOURNAL
Vol. 36, No. 8, August 1998

Microgravity *n*-Heptane Droplet Combustion in Oxygen–Helium Mixtures at Atmospheric Pressure

V. Nayagam,* J. B. Haggard Jr.,† and R. O. Colantonio‡
NASA Lewis Research Center, Cleveland, Ohio 44135
A. J. Marchese§ and F. L. Dryer¶
Princeton University, Princeton, New Jersey 08544
and
B. L. Zhang** and F. A. Williams††
University of California, San Diego, La Jolla, California 92093

Results are presented from experiments on the combustion of freely floated *n*-heptane droplets in helium–oxygen environments conducted in Spacelab onboard the Space Shuttle Columbia during the first launch (STS-83) of the Microgravity Science Laboratory mission in April 1997. During this shortened flight, a total of eight droplets were burned successfully in nominally 300 K oxygen–helium atmospheres having oxygen mole fractions of 25, 30, and 35% at a total pressure of 1 atm. Initial droplet sizes ranged from about 2 to 4 mm. The results demonstrated both radiative and diffusive flame extinction during burning, whereas droplet surface regression followed the *d*-square law. The full range of possible droplet-burning behaviors was thus observed. The results provide information for testing future theoretical and computational predictions of burning rates, soot and flame characteristics, and extinction conditions.

Introduction

ADVANCEMENT of basic understanding generally is served best by studying well-defined problems. Isolated, single-droplet burning is the simplest example of nonpremixed combustion that involves participation of a liquid phase (the fuel) in addition to the gas-phase diffusion flame. Investigation of the combustion of a single, isolated liquid droplet affords the opportunity to study the interactions of physical and chemical processes in an idealized and simplified geometrical configuration. The insights gained from such investigations can then be applied for improving means of burning liquid fuels with greater efficiency, cleanliness, and safety.

The experimental apparatus described is designed for studying droplets having initial diameters between 1.5 and 5.0 mm. These dimensions aid in measurement by circumventing spatial resolution difficulties encountered for smaller droplets and expose phenomena such as influences of radiation energy loss, which are not significant at smaller sizes under ordinary atmospheric conditions. In normal gravity, however, combustion of these larger droplets is strongly influenced by natural buoyant convection, which destroys the desired spherical symmetry. Microgravity provides a means for greatly reducing these convective effects and, thus, achieving geometrical simplification that facilitates analysis and understanding of the results.

Kumagai[1] pioneered the use of microgravity in studying droplet combustion. His drop tower provided about 1 s of microgravity, enabling him to burn to completion droplets of initial diameters slightly less than 1 mm. Numerous droplet-combustion drop-tower and parabolic-flight studies of this type have since been performed.[2–34] To emphasize the large extent of this work, it may be noted that the first 34 references all report some microgravity experimental results but yet represent only part of the wide-ranging experimental droplet-combustion research that has now been done in microgravity. The well-known *d*-square law of droplet combustion, namely, that the square of the droplet diameter decreases linearly with time, indicates that, in the largest drop tower available (the 10-s tower in Hokkaido, Japan), droplets up to about 3 mm in initial diameter can be burned to completion. Because aircraft flying parabolic trajectories fail to produce the low-gravity levels (10^{-4}–10^{-6} Earth gravity) needed to eliminate buoyant influences in spherical droplet burning (calculated by considering influences of droplet displacement, velocity, and acceleration in the conservation equations and by requiring the droplet to remain in the field of view of the droplet imager for the entire burning history) and because droplet-combustion experiments in sounding rockets would be fairly ambitious and expensive to design, Spacelab offers an attractive opportunity to study the combustion of large droplets. Although Spacelab experiments also are expensive, they offer advantages in that a number of experiments can be performed in one flight, and results of early experiments can be used to decide what later tests need to be done.

Droplet combustion experiments were performed in one previous Spacelab flight,[35] the second U.S. Microgravity Laboratory mission, aboard the STS-73 launch of the Space Shuttle Columbia. That set of experiments employed the small, multiuser glove box facility, necessitating development of a simplified approach to droplet suspension. The apparatus adopted fine fibers to support droplets ranging in initial diameter from about 2 to 5 mm. This fiber-supported droplet combustion (FSDC) experiment also was flown on the STS-83 mission discussed here, but the shortened flight did not permit execution of any FSDC-2 droplet-burning tests. The FSDC experiments on STS-73 did provide a considerable amount of information concerning the burning of droplets of methanol and of heptane–hexadecane mixtures in air, but no data were obtained for heptane droplets that could be compared with the results reported here. Two limitations of the FSDC experiments are that combustion can be investigated only in Spacelab cabin air environments and that the fiber support can cause perturbative departures from spherical symmetry during combustion. The free-droplet studies here reported eliminate any fiber effects and allow the pressure and composition of the atmosphere in which the droplet combustion occurs to be adjusted as desired, thereby providing greater flexibility. Improvements in the diagnostic instrumentation also provide greater fidelity of the experimental measurements.

Received Oct. 17, 1997; revision received March 9, 1998; accepted for publication March 9, 1998.

*Principal Researcher, National Center for Microgravity Research.
†Project Manager, Droplet Combustion Experiment.
‡Aerospace Engineer.
§Graduate Student, Department of Mechanical and Aerospace Engineering. Member AIAA.
¶Professor, Department of Mechanical and Aerospace Engineering. Member AIAA.
**Graduate Student, Department of Applied Mechanics and Engineering Sciences. Member AIAA.
††Professor, Department of Applied Mechanics and Engineering Sciences, and Director, Center for Energy Combustion and Research. Fellow AIAA.

In the present experiments, *n*-heptane was selected as the fuel, and mixtures of helium and oxygen, with different oxygen percentages and different total pressures, were employed as the atmosphere in which the droplet combustion occurs at normal cabin temperature. The many recent studies of *n*-heptane combustion and chemical kinetics,[36–42] following from heptane's adoption by much of the scientific community as an attractive model pure fuel for obtaining basic information relevant to combustion in practical engines, especially diesels, motivated the choice of this fuel for the present work. Many heptane–air droplet-combustion experiments have been performed in drop towers (so many that heptane almost has become a standard fuel for droplet-burning studies), and to facilitate direct comparisons with this extensive database, it would be of interest to employ oxygen–nitrogen mixtures as the oxidizing environment in Spacelab experiments. The selection of helium rather than nitrogen as the diluent in the present experiments was based on a number of considerations. Experimental and computational results indicated that the use of helium reduces sooting, increases burning rate, and leads to flame extinction at larger droplet diameters, thereby improving the ease with which accurate measurements can be made. The higher thermal diffusivity of helium plays an important role in achieving these benefits. Although no heptane droplet-combustion experiments have previously been performed in helium–oxygen mixtures (other than the exploratory experiments run in developing the present Spacelab experiments), systematic drop-tower experiments can readily be performed in the future, for initial droplet diameters below about 1.5 mm, to provide comparisons with the Spacelab results on large droplets. Additional interest in helium dilution stems from its potential use in increasing fire safety.

This paper presents initial results from experiments on free-floated *n*-heptane droplet combustion conducted at a total pressure of 1 atm in three different oxygen–helium environments onboard the STS-83 flight of the Space Shuttle Columbia during the first Microgravity Science Laboratory mission (MSL-1). The general purpose of these experiments is to produce data over a wide range of initial conditions, which will provide a basis for refining existing phenomenological understanding of droplet burning and extinction processes and permit quantitative assessment of our theoretical ability to predict these phenomena. These data are to be utilized specifically to test theoretical predictions of liquid-phase and gas-phase steady and unsteady phenomena and of flame-extinction phenomena in the spherically symmetrical burning of a pure fuel droplet. Through study of larger droplets than have been tested previously, the range of characteristic times over which chemical–kinetic influences can be investigated is increased. Unanticipated phenomena might also occur at these longer times.

Experimental Approach

The experiments were conducted in the droplet combustion experiment (DCE) apparatus located in rack 8 within the Spacelab facility, in the cargo bay of the Space Shuttle Columbia. Rack 8 was chosen for the DCE because it is located close to the center of gravity of the Space Shuttle and, thus, produces low residual gravity levels compared to other rack locations. The primary components of the DCE apparatus are the combustion chamber, the internal apparatus, the diagnostic system, and the gas-supply system. The combustion chamber is a 346-mm-long cylindrical section with a 342.9-mm inside diameter, manufactured from 6061-T6 aluminum. The cylinder heads are elliptical with a 2:1 ratio. The combustion chamber has an internal volume of 42.4 liters. The internal apparatus, shown in Fig. 1, is mounted inside the combustion chamber and contains the droplet-deployment mechanisms, two diametrically opposed hot-wired igniters, a fuel-supply system, and a gas-mixing fan. The droplet-deployment system consisted of two L-shaped hypodermic needles (outer diameter 0.254 mm) made of stainless steel, mounted horizontally on the shafts of the two dc motors. These servo motors are placed in such a manner that the needle tips meet tangentially, from opposite directions, when they are brought together. The needle tips were flared slightly (flare diameter 0.341 mm) so that the fuel droplet generated between the needles is centered and held in place when the needles are stretched prior to deployment. Droplets are deployed freely by injecting a metered amount of fuel between the tips of the two needles, stretching the droplet slightly and then withdrawing the needles simultaneously at a high acceleration. At the moment that a droplet is deployed, the hot-wire igniters are activated to initiate combustion of the freely floating droplet, and they are then withdrawn slowly away from the region of combustion. The precise positioning of the needles and the timing of the sequence of events are controlled by the experiment control computer (ECC), a microprocessor located within the DCE avionics compartment.

Figure 2 shows the DCE primary diagnostic system, which consists of a 35-mm, high-speed motion-picture camera that captures the back-lit images of the droplet (droplet-imaging camera in Fig. 2) and an intensified-array camera with an orthogonal view that images the ultraviolet (uv) emission arising from the hydroxyl-radical chemiluminescence in the flame zone (flame-imaging camera in Fig. 2). In addition, a standard color video camera is used to monitor the experiment operations within the combustion chamber. The back lighting for the droplet-view camera is provided by a collimated beam from a red-light-emitting diode light source. The field of view for the high-speed droplet-view camera is a 30×30 mm area centered around the deployment location. The high-speed camera is run at 80 frames/s, and the black-and-white images are recorded on a Kodak Teck Pan film. A telecentric lens system is used with

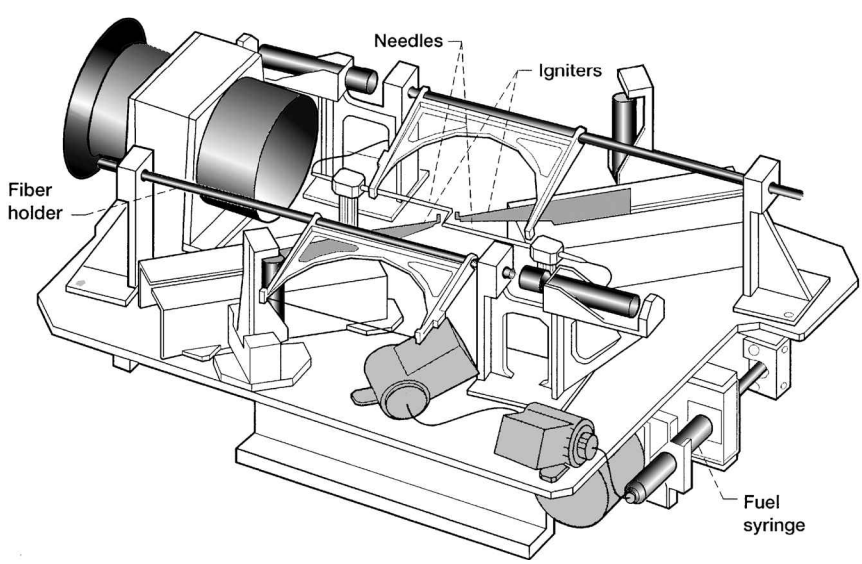

Fig. 1 Schematic diagram of the internal apparatus of the DCE.

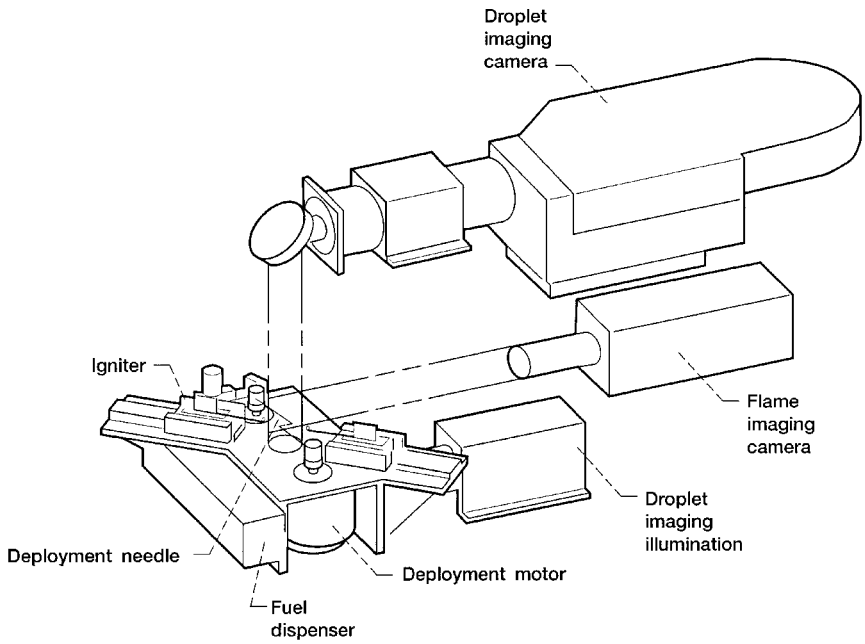

Fig. 2 Schematic diagram of the DCE primary diagnostic system.

the high-speed camera to minimize the magnification factor when the free-floating droplet moves in and out of the field of view. The optics and the development processes for the 35-mm film are optimized to obtain an edge resolution up to 18 μm. The flame-view charge-coupled device camera, located along an axis perpendicular to the droplet-view camera, has a field of view of 50 × 50 mm, and its imaging optics consist of a 50-mm uv-transmissive lens and a narrow-band interference filter centered at 310 nm. The uv images are taped on a Hi-8 video recorder and have a standard video time resolution of 30 frames/s or 60 fields/s. Both the droplet images and the uv flame images are time-stamped accurate to 1/1000 of a second so that they can be time correlated during data analysis. A crew-view port in the combustion chamber allows the crew member to monitor the experiment visually or, alternatively, to take 35-mm still, color pictures of the burning droplet using a Nikon F4 camera.

The temperature and pressure in the combustion chamber are also monitored, in this case at a rate of 10 Hz, throughout an experimental run by the ECC, and the data are stored in onboard memory units. The ECC forms the heart of the DCE avionics. Besides controlling the droplet-deployment servo-motors and their optical encoders, the ECC controls the fuel-syringe stepper motor and the linear stepper motors for the hot-wire igniters. It also forms the interface for crew commanding of the experiment by a lap-top computer or for ground-control commands, so that the droplet deployment and ignition processes can be accomplished either by the crew or by ground commanding. During the STS-83 flight, two burns were run by ground command; the rest were run by a crew member onboard.

Experiment initial conditions are first established by venting the combustion chamber to space vacuum and then filling it with a premixed gas bottle containing the required oxygen–helium mixture. The gas bottles are filled on the ground in such a manner that, when they are emptied into the evacuated DCE combustion chamber, the desired ambient pressure and oxygen concentrations are established. Because several burns are conducted in a given environment, the postcombustion environment is sampled for ground analysis by using an evacuated bottle prior to venting. This improves the precision in determining the environment in which each droplet is burned. A Shuttle crew member initiates a chosen experimental run by positioning the droplet-deployment needles and the hot wire at a predetermined home position prior to the start of an experimental run. The process of injecting a measured amount of fuel, stretching the needles, and then deploying the droplet is accomplished by using commands from the lap-top computer connected to the ECC. The igniters are then energized for a predetermined time period and then withdrawn slowly away from the deployment site. The stretched position of the deployment needles prior to deployment, the position of the hot-wire igniters relative to the droplet surface, and the precise timing between dispense, deployment, and ignition are predetermined based on theoretical calculations for stretched droplet shapes and droplet evaporation rates; extensive ground-based tests were carried out in the NASA Lewis Research Center 5-s drop tower to refine the parameter selections. The 35-mm, high-speed film camera and the uv camera are activated just before the automated sequence of droplet stretch, deployment, and ignition.

The research-grade (99% purity) *n*-heptane fuel used in this study was obtained from a commercial vendor and was degassed prior to loading in the fuel syringe for approximately three months before being installed in the combustion vessel. The fuel composition was analyzed before and after the flight, and negligible (much less than 1%) changes were found in fuel composition.

Data Reduction and Results

The principal data are obtained from the back-lit images of the droplet and OH-chemiluminescent images of the flame. Figure 3, an example of the former, shows the sequence of events in an experimental run. The first frame shows the droplet formed on the needles prior to stretching and the pair of hot-wire igniter loops in place. In the second frame, the droplet has been stretched and is ready for deployment. The third frame, taken just after needle extraction, is at the time of maximum amplitude of liquid oscillation. The next frame shows the beginning of the soot buildup during ignition; the soot flows outward along the axis of the loops but avoids the hot wires themselves because of thermophoretic and/or gas-flow effects. In subsequent frames, the igniters have been retracted, and the histories of the soot shell and droplet diameter can be traced. Noteworthy are the clarity with which individual soot agglomerates can be seen, the gradual decrease in soot-shell elongation toward the retracted igniter axis, and the decrease in soot density with increasing time.

As a consequence of the shortened mission, only eight successful runs were carried out, all at 1 atm and with three different oxygen–helium mixtures. The droplet initial sizes were between 1.7 and 4.1 mm. Results of analyses of all frames of the droplet-view and flame-view images are shown in Figs. 4–6 in terms of histories of diameter squared for each of the three different atmospheres. Table 1 summarizes the test atmospheres, the initial droplet diameters d_0 employed in analysis, the burning-rate constants K derived from the data, and the average droplet drift velocities V measured from the back-lit film. The ways in which these values were obtained are described subsequently. The numbering of the experimental runs, given in Table 1, is selected for convenience in describing the results and reflects neither the designations employed during the experiments nor the order in which the experiments were performed.

The back-lit images of the droplets and the OH-chemiluminescent images of the flame were digitized and analyzed using a personal computer-based image-analysis system.[43] The system identifies edge locations on the basis of gradations in intensity. This procedure is most accurate for droplets later in the burning history; initially the relatively heavy sooting makes edge determination more difficult. For the data shown in Figs. 4–6, the reported diameters are those of a circle having the area measured by the image-analysis system. The small-scale irregularities visible in figures are representative of inaccuracies associated with the image resolution and analysis. For the droplets, the results were checked by visual measurements of some film frames and by direct measurement of two orthogonal diameters using the image-analysis system. Accuracies of droplet diameters were inferred from these results to be better than 5%. The flame images almost always were observed to be quite round with well-defined edges. Profiles of OH are to be obtained by deconvolution of the flame-image intensities, but because this analysis has not been completed, only the outer flame diameters are reported here. These outer diameters are essentially diameters of maximum flame-image intensities because at the edge the intensities fall rapidly from the maximum to zero. From the flame and droplet diameters, the flame standoff ratio, that is, the ratio of the flame diameter to the droplet diameter, can be computed directly. Figure 7 shows these ratios as functions of time for all eight experimental runs.

From the back-lit views, such as those of Fig. 3, the soot particles are quite visible. The outer boundary of the soot cloud is rather well defined in these photographs. Although the major diameter of

Table 1 Experimental conditions, measured burning rates, and average drift velocities

Run no.	O_2%	d_0, mm	K, mm^2/s	V, mm/s
1	35	1.9	1.34	4.17
2	35	3.1	1.21	1.70
3	35	4.1	1.19	1.54
4	30	3.2	1.02	1.99
5	30	3.9	1.02	1.09
6	25	2.8	0.91	1.12
7	25	3.2	0.94	0.90
8	25	4.1	0.99	1.62

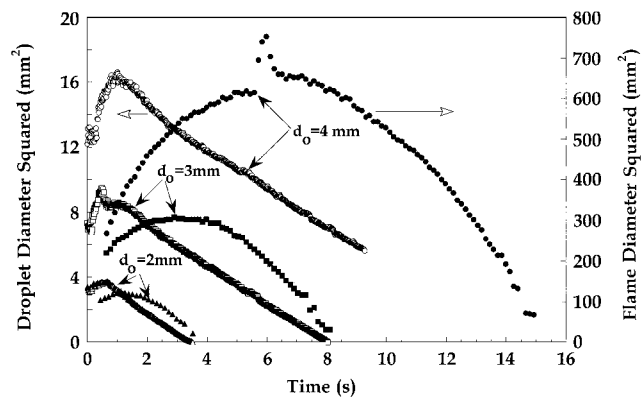

Fig. 4 Square of the droplet and flame diameters as functions of time for an ambient oxygen–helium environment having an oxygen mole fraction of 35% at 1-atm pressure.

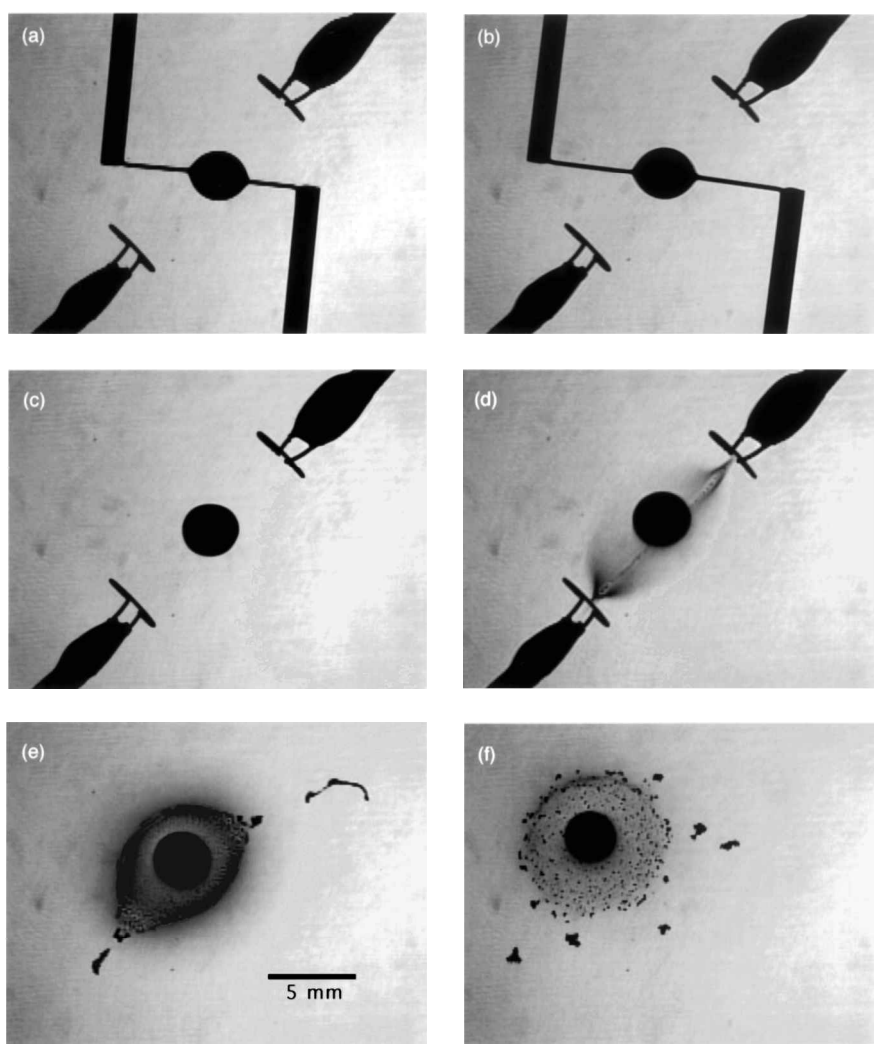

Fig. 3 Selected back-lit frames for the 4-mm droplet in 35% oxygen, showing deployment, ignition, and subsequent combustion.

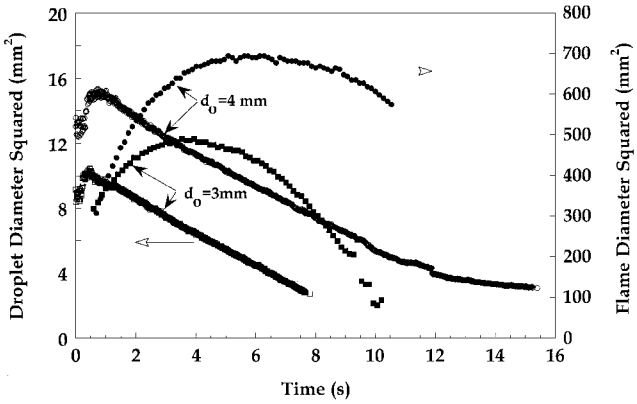

Fig. 5 Square of the droplet and flame diameters as functions of time for an ambient oxygen–helium environment having an oxygen mole fraction of 30% at 1-atm pressure.

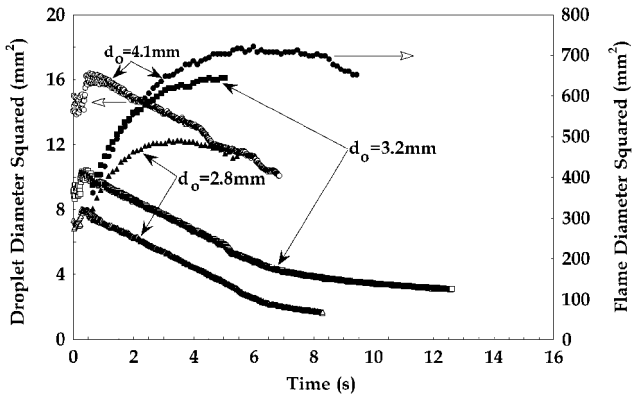

Fig. 6 Square of the droplet and flame diameters as functions of time for an ambient oxygen–helium environment having an oxygen mole fraction of 25% at 1-atm pressure.

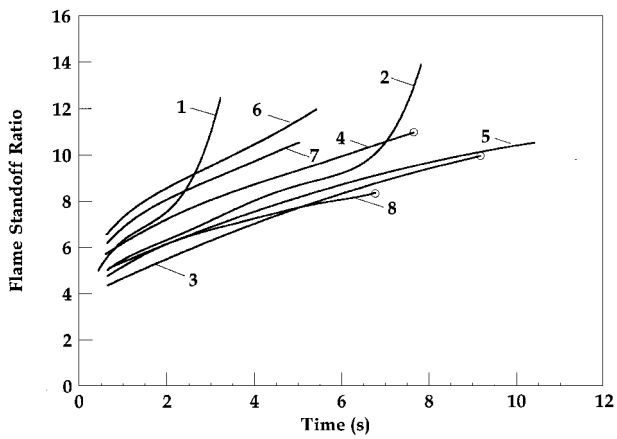

Fig. 7 Flame standoff ratios as functions of time.

this cloud is influenced by initial conditions and initially decreases rapidly with time, the minor diameter seems fairly representative of a spherical combustion process. Figure 8 shows the ratio of this minimum outer soot-cloud diameter d_s to the liquid droplet diameter d_l as a function of the scaled time t/d_0^2. Data on this figure were taken from all eight runs at 1- or 0.5-s time intervals. Additional soot-particle information, such as distributions of number densities and sizes and shapes of soot particles and agglomerates, remain to be extracted from the back-lit films.

For later investigation of the effects on the burning-rate constant K of the Reynolds number Re, the relative velocity of the droplet with respect to the gas is needed. For this purpose, the relative velocity may be taken to be the drift velocity V reported in Table 1. This velocity was obtained from the image-analysis system[43] by

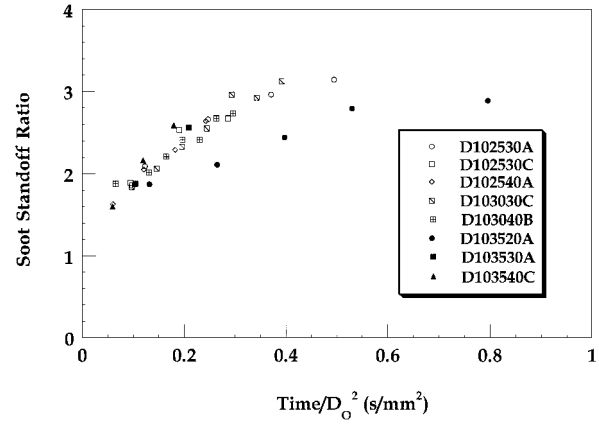

Fig. 8 Soot standoff ratios as functions of time.

tracking the centroid of the droplet area and the flame area. Because the droplet and flame views are orthogonal, droplet drift in three dimensions is obtained by assuming that the droplet is in the center of the flame. Most of the droplet motion is in the droplet view because the droplet-view camera is located along an axis perpendicular to the droplet deployment plane, the plane within which the deployment needles and igniters move. Deployment and ignition imbalances generate droplet velocities in this plane, although those velocities were observed to be appreciably smaller than velocities in most earlier experiments, namely, on the order of 1 mm/s rather than 10 mm/s. The droplet drift velocity could be larger or smaller than the relative velocity that belongs in Reynolds number because the gas need not be at rest, but gas velocities were calculated to be small as a consequence of allowing sufficient time for gas currents to dissipate prior to initiating an experimental run. In most runs, the drift velocities were found to be nearly constant, but in 35% oxygen, where droplets burned to completion, sudden droplet accelerations were observed near the end of combustion for reasons that are still under investigation. The 3.0-mm depth of field of the droplet-imaging camera was sufficient to maintain negligible (less than 20-μm) error in droplet-diameter measurements associated with droplet motion.

Discussion of Results

The results shown in Figs. 4–6 span the full range of droplet-combustion behavior. In all of these figures, time is measured starting from the first frame following withdrawal of the deployment needles, and droplet and flame views are synchronized within 0.1 s through Greenwich mean time stamps. Needle withdrawal induces droplet oscillations in the first spherical harmonic mode. These oscillations are evident in the back-lit images, and amplitudes and frequencies may be extracted from those images in the future because the frame-to-frame time reduction is sufficient for that purpose. The long timescales in Figs. 4–6 cause the oscillations to appear as scatter at the beginning. The oscillation amplitude and duration increase with increasing droplet size. In all cases, oscillation amplitudes are viscously damped to immeasurable values in less than 1 s. Ignition occurs between 0.3 and 0.5 s after deployment, with the longer time corresponding to the larger droplets, as can be seen from Fig. 4, where the first flame-diameter points mark ignition. Only for the largest droplets did oscillations persist through ignition. The hot-wire ignition was not observed to induce any droplet oscillation or motion. This stands in contrast to spark ignition, which can cause droplet oscillation and movement,[21,44] although perhaps not significant movement for the larger droplets studied here.

The droplet diameter increases during ignition; the initial value reported in Table 1 is the maximum value achieved after this expansion. The coefficient of thermal expansion of heptane produces about an 11% increase in volume between ambient temperature and boiling temperature, corresponding to a 7% increase in d_l^2. Although this is consistent with data in Fig. 4 for $d_0 = 2$ mm, the initial expansion of the other two droplets in Fig. 4 appreciably exceeds this estimate. The reason for the difference is believed to be chamber-atmosphere gas initially present within the liquid. For the 3-mm droplet in Fig. 4,

a small gas bubble is observed to burst during ignition and to produce the dip in the droplet-diameter trace shortly before 1 s; for the largest droplet the gas desorbs gradually over a period of about 2 s. These gas-dissolution effects are weaker in Figs. 5 and 6, and in no cases are they significant after 2 s.

35% Oxygen

The data for the richest oxygen environment, shown in Fig. 4, exhibit nearly classical behavior after the initial transients. The square of the droplet diameter decreases essentially linearly with time, all the way to zero diameter. The largest droplet passes out of the field of view of the back-lit camera at the time that its droplet-diameter data in the figure end, but the flame remains sufficiently in the field of the flame-view camera for the entire combustion history. Similar behavior occurs for one droplet in Fig. 5 and for one in Fig. 6; in all cases, the flame view recorded the entire combustion history.

Unlike the droplet diameter, the flame diameter gradually increases and then decreases during d-square burning. This is consistent with calculated influences of the outer transient region that surrounds the quasisteady region during droplet combustion.[45,46] The surface regression of liquid is controlled mainly by the inner quasisteady convective–diffusive region of the gas adjacent to the liquid, giving rise to the d-square behavior in the first approximation, but there are perturbations associated with the perpetually outward isotherm movement in an outer transient-diffusive regime. A small parameter for matched asymptotic expansions can be defined as

$$\epsilon = (\rho_\infty/\rho_l)^{\frac{1}{2}} \tag{1}$$

where ρ denotes density and the subscripts ∞ and l the ambient gas and the liquid, respectively. The length scale in the inner region is of the order of the droplet diameter, whereas that in the outer region is larger by the factor ϵ^{-1}. The processes occurring in the outer region produce perturbations of order ϵ on the solutions in the inner region.[45]

For illustrative purposes, approximate all gas-phase diffusivities by a constant D_g. The classical burning time of a droplet is then

$$t_b = \frac{d_0^2}{8D_g\epsilon^2\,\ell n(1+B)} \tag{2}$$

where B denotes the transfer number. Including the first perturbation from the outer transient zone results in[45]

$$\left(\frac{d_l}{d_0}\right)^2 = 1 - \frac{t}{t_b'} + \frac{d_0}{\sqrt{4\pi D_g t_b}} F\left(\frac{t}{t_b'}\right) \tag{3}$$

where

$$F\left(\frac{t}{t_b'}\right) = \frac{t}{t_b'} - \sqrt{\frac{t}{t_b'}} - \frac{1}{2}\left(1-\frac{t}{t_b'}\right)\ell n\left(\frac{1+\sqrt{t/t_b'}}{1-\sqrt{t/t_b'}}\right) \tag{4}$$

and the corrected burning time is

$$t_b' = \frac{t_b}{1+\epsilon\sqrt{(2/\pi)\,\ell n(1+B)}} \tag{5}$$

The ordinary d-square law is expressed by the first two terms on the right-hand side Eq. (3). Use of the solution to Eq. (2) for d_0 on the right-hand side of Eq. (3) clearly demonstrates that the remaining term on the right-hand side of Eq. (3) is a correction of order ϵ. Because the value of ϵ in these experiments is only a few percent, that reduction in the burning time is small, although the logarithmic singularity causing $d(d_l)^2/dt$ to approach zero as t approaches t_b' might be reflected in the last few droplet-diameter points in Fig. 4 for $d_0 = 2$ mm. By contrast, the influence of this perturbation on the flame-diameter history is large.

The history of the flame diameter depends quantitatively on whether the flame is located in the inner or outer zone. Although it is in the outer zone for sufficiently high dilutions of the atmosphere, estimates indicate that it should spend most of its life in the inner zone in these experiments, especially for Fig. 4. The classical quasisteady ratio of flame to droplet diameter (the flame standoff ratio) is

$$r = \frac{\ell n(1+B)}{\ell n\left(1+Y_{O_2\infty}/\nu\right)} \tag{6}$$

where ν denotes the mass of oxygen consumed per unit mass of fuel burnt and Y_{O_2} the mass fraction of oxygen. The first perturbation to the flame position when it is located in the inner region is[45]

$$\frac{d_f}{d_l} = r\left[1 + (r-1)\frac{d_0}{4\sqrt{\pi D_g t_b}} G\left(\frac{t}{t_b'}\right)\right] \tag{7}$$

where

$$G\left(\frac{t}{t_b'}\right) = \ell n\left(\frac{1+\sqrt{t/t_b'}}{1-\sqrt{t/t_b'}}\right) - \frac{2}{\sqrt{t/t_b'}} \tag{8}$$

Here the perturbation of order ϵ diverges as t approaches zero and also (logarithmically) as t approaches t_b. These divergences lead to appreciable departures of the flame location from its quasisteady position, giving a small flame radius at early times and always forcing the flame into the outer region just prior to burnout. The flame-diameter histories in Fig. 4 are qualitatively consistent with these predictions. Quantitative comparisons were not made because of the constant-property approximations in the theory, although published theoretical flame histories[45] qualitatively resemble the experimental results. By extending recent work,[46] it may be possible to account for variable properties accurately in the asymptotic analysis when the flame is in the outer region. Numerical modeling approaches[31] can account for variable properties irrespective of whether the flame is in the outer region; both approaches are worthwhile and can help to make quantitative comparisons with experiment. Qualitatively similar behavior also has been obtained from a simplified numerical model,[47] which could be tested quantitatively against these experiments.

If the flames were in the inner quasisteady zone and unperturbed by the outer transient zone, then the square of the flame diameter would decrease linearly with time. This clearly does not happen in Fig. 4, except possibly toward the end of each burn. Within the accuracy of the data, the flame-diameter curves approach straight lines that reach zero at approximately the same time that the droplet-diameter curves reach zero (the extrapolated droplet-diameter curve for $d_0 = 4$ mm). This indicates that the last term in Eq. (8) is the main cause of the observed departure of flame diameter from quasisteady behavior. The flame standoff ratio is, however, a more sensitive indicator of achievement of a quasisteady flame position. The standoff ratios for runs 1 and 2, shown in Fig. 7, resemble those published previously[45] and suggest that these ratios passed through the quasisteady value quickly, near the inflection point, indicating that quasisteady conditions were not achieved, the first term in Eq. (8) becoming important at the end of the burn. The large circle at the end of run 3 (and also runs 4 and 8) in Fig. 7 marks the passage of the droplet from the field of view, an event that prevents late-time standoff ratios from being obtained. The data that do exist for run 3 are, however, consistent with those of runs 1 and 2 and suggest approximate universal scaling if the time were normalized by t_b, in agreement with predictions from Eqs. (2), (7), and (8).

The flame-view camera records a nonzero flame diameter in the last frame before complete flame disappearance. This diameter corresponds to the last flame-diameter data point of each run in Fig. 4 and will be referred to as the flame diameter at extinction d_{fe}. Although values of d_{fe} in Fig. 4 are too small to measure with much accuracy, they do appear to increase somewhat with increasing initial droplet diameter d_0 (although this is not totally certain for the 4-mm droplet because in that case the last flame view is at the edge of the frame). Variation of d_{fe} with d_0 is inconsistent with previous theory[36–38] for pure heptane droplets, which postulated quasisteady behavior up to conditions of flame extinction through reduction of Damköhler numbers, so that d_{fe} is independent of d_0.

These extinctions appear to be diffusive in the sense that the heat loss that reduces the flame temperature is conductive. The quasisteady theories[36–38] expressed results in terms of droplet diameters at extinction d_{le} rather than d_{fe}, but by use of r of Eq. (6) they can

readily be expressed in terms of d_{fe}. Because the chemistry responsible for extinction occurs at the flame, in a sense d_{fe} is of more fundamental relevance than d_{le} as a measure of the time available for chemistry to occur. It would be necessary to use d_{fe} instead of d_{le} here because d_{le} is too small to measure. In fact, within the accuracy of the timing in Fig. 4, it is impossible to determine whether the flame extinguishes before or after the droplet disappears; either of these two situations is possible theoretically, depending on how reactive the fuel vapors are, and in Fig. 4 the two events seem to occur almost simultaneously. Although the extinctions must be diffusive for these small flames, the quasisteady approximation appears to be inapplicable because d_{le} is practically zero, whereas d_{fe} is not; the extinctions seem to occur after the flame has moved into the outer zone. Diffusive extinction analyses have not yet been worked out for flames in the outer transient zone, but the requisite asymptotic theory can readily be developed, as should be done for comparison with these experimental results, as well as computational predictions.

The irregularity in the flame-diameter trace in Fig. 4 for $d_0 =$ 4 mm may be due to ignition of a large soot aggregate passing through the flame; there is a consequent nonspherical outward bulge of flame luminosity that leads to the abrupt brief increase in the area-average flame diameter at about 6 s into the burn, with very little resulting influence on the droplet shape or diameter history. This explanation relates to the sooting tendency, to be discussed more fully later, which is much more severe in this oxygen-rich atmosphere than in the other atmospheres. The soot particles form and aggregate in a hot fuel-rich region inside the flame at a diameter appreciably smaller than the flame diameter.[23] After the growing soot particles become large enough that thermophoretic forces no longer can balance the Stefan-flow drag, the soot is transported outward through the flame by the flow, and the largest particles can be ignited as they pass through the flame.

The droplet-diameter curves in Fig. 4 are slightly convex downward, in contrast to the concavity typically observed for heptane droplet combustion[17,22] and often attributed to gradual droplet heat up. In other words, just as with methanol,[35] the burning-rate constant seems to decrease slightly rather than increase with time. For methanol, this behavior is known to be associated with water absorption during combustion, but water does not dissolve to any appreciable extent in heptane. Although various hypotheses have been put forward for explaining the curvature, the true source of these small departures from linearity in Fig. 4 remains a topic for future study.

30% Oxygen

The two burns represented in Fig. 5 exhibit very different behaviors. The smaller droplet, which leaves the back-lit field of view at about 8 s, burns very much like the droplets in 35% oxygen; the classical d-square history and flame expansion and then contraction are evident. Extrapolation of the droplet-diameter curve indicates that this droplet would disappear very near the time of flame extinguishment. The extinction again is diffusive at a small but now reasonably measurable flame diameter. An interesting open question concerns whether this occurs in the quasisteady regime, that is, whether there would have been a measurable droplet diameter at extinction. The greater dilution of the atmosphere, in comparison with 35% oxygen, will greatly slow the gas-phase combustion chemistry and thereby produce earlier flame extinction, possibly during quasisteady burning for both droplet and flame.

For the larger droplet, however, flame extinction occurs well before the droplet diameter approaches zero; in fact, it occurs at nearly the maximum flame diameter. This extinction cannot be diffusive because the rate of conductive heat loss from the flame is larger earlier in the flame history, when the flame diameter is smaller. During this period, the diffusive energy loss rate is greater; that is, the tendency toward diffusive extinction is greater, but the flame is observed to be strong, without tendency toward extinction. Radiant energy loss from the flame is known to lead potentially to flame extinction[48] and has been documented for the combustion of larger methanol droplets in air.[35] There are both maximum and minimum diameters beyond which combustion does not occur,[49] the energy loss being diffusive at the minimum diameter and radiative at the maximum. The data for the larger initial diameter in Fig. 5 represent the first documented radiant extinction for heptane droplet combustion.

Because the gas is nearly transparent, the total rate of radiant energy loss from the flame is proportional to d_f^3. The strong increase in emissivity with temperature enables radiant loss rates to be treated universally through asymptotic analysis.[50] Infrared band emissions from H_2O and CO_2 are major contributions to the radiant loss,[51] and the necessary band emissivities are available.[51,52] Although heptane experiences radiant energy loss from soot as well, numerical modeling[51] has shown that the radiant loss reduces flame temperatures appreciably for larger droplets and thereby may reduce sooting and radiant energy loss from soot in the present experiments so that the band radiation may still be dominant, as it is for methanol.[51] The radiant energy loss rate must be compared with the diffusive rate of heat generation by combustion in developing radiant extinction criteria. Because this diffusive rate is proportional to d_f^2, the tendency toward radiant extinction increases in proportion to d_f. It, therefore, may be expected that, as the flame diameter grows with time, a diameter may be reached at which extinction occurs through radiant loss. This explains why the larger droplet in Fig. 5 can experience radiant extinction, whereas the smaller one does not; the flame of the smaller droplet does not become sufficiently large. Radiant extinction may occur slightly after the maximum flame diameter is reached, as occurs in Fig. 5, because the diffusive rate of heat release is decreasing with time as a consequence of the decreasing droplet diameter.

Analyses of radiant extinction can parallel earlier analyses of diffusive extinction insofar as chemical kinetics are concerned. Radiant energy loss must, however, be included, and the flame motion cannot be treated as quasisteady. Time-dependent, spherically symmetrical numerical computations are well suited for such calculations.[30,51] Asymptotic analyses could employ rate-ratio asymptotics in the innermost flame zone, flanked by radiant-loss zones,[50] with Eq. (7) applied for the time-dependent flame diameter and the associated mixture-fraction field needed for the scalar dissipation. Analyses of this last type would be worthwhile to pursue but have not been completed. The continuing evolution of the mixture-fraction field that would be calculated from such theories could well predict extinction not exactly at the maximum flame diameter but rather shortly after the flame has begun to shrink slightly, as observed in Fig. 5.

It is noteworthy that, for $d_0 = 4$ mm in Fig. 5, quasisteady d-square droplet-diameter behavior occurs for a long time, nearly 10 s, prior to flame extinction. This emphasizes how remarkably decoupled the droplet and flame process are. The slight downward convexity of the droplet curves, identified previously for 35% oxygen, is also seen during this quasisteady burning for the larger droplet in Fig. 5. After extinction, the droplet evaporation rate is seen in Fig. 5 to decrease more noticeably, as expected. This decrease is, however, less abrupt than for methanol droplets.[19,35] The larger flame standoff ratio for heptane results in more energy being left in the gas after extinction and a consequent more gradual decrease in vaporization rate.

The experiments reveal a number of interesting aspects of the dynamics of soot particles. These particles normally migrate around the soot-diameter position as they aggregate and eventually move out through the flame. The soot passing through the flame is very evident in the back-lit view because the particle velocity rapidly increases after the particle traverses the reaction zone as a consequence of the suddenly favorable temperature gradient for enhancing the outward thermophoretic velocity, in contrast to the retarding thermophoretic effect for particles inside the flame. The lower gas density in the vicinity of the flame also helps to increase velocities there. Soot particles, thus, are helpful markers of gas motion once thermophoretic effects are subtracted; temperature gradients can be inferred from thermopherotic effects.

A distinctive behavior of the soot particles associated with flame extinction was observed most clearly in 30%-oxygen atmospheres. When the flame extinguishes, all soot particles move inward rapidly toward the droplet and then turn around and gradually move outward, eventually becoming essentially stationary. This behavior is qualitatively consistent with predictions by an asymptotic analysis of the history of gas motion produced by extinction of the diffusion flame around a droplet.[53] The gas-density increase associated with the temperature decrease after extinction gives rise to the inward motion, whereas the continuing slow droplet vaporization causes the subsequent outward motion. Because of the theoretical idealizations

and anticipated experimental inaccuracies, quantitative comparisons were not attempted.

The flame-standoff curves for runs 4 and 5 in Fig. 7 are of similar shape and would correlate better with t/t_b, as discussed earlier for 35% oxygen. If the 3-mm droplet had not passed out of the field of view, its flame-standoff curve (run 4) might have developed an inflection like those seen for runs 1 and 2. The radiant extinction precludes an inflection for run 5.

25% Oxygen

All three flames in Fig. 6 experience radiant extinction like that seen for the larger droplet in Fig. 5. The 30%-oxygen concentration, thus, approximately provides the boundary between diffusive and radiant extinction. Only in that atmosphere did the smaller flame extinguish diffusively and the large one radiatively. In 25% oxygen, the lower peak temperatures have reduced the chemical rates to such an extent that flames of all sizes measured extinguish radiatively. The corresponding flame-standoff curves for runs 6 to 8 in Fig. 7 have no inflection and would correlate to a clearly larger flame-standoff ratio than for 35% oxygen, as would be expected from the stoichiometry according to Eq. (6).

It is seen from Fig. 6 that there is a tendency for larger droplets to have their flames persist for a longer time (although some possible departure from this behavior is seen for the two smaller droplets). A correlation of this type is expected from Eq. (7) because of the appearance of the time dependence through t/t_b. In weak atmospheres, extinction occurs early enough that the initial outward diffusion transient is dominant, and Eqs. (7) and (8) become approximately

$$\frac{d_f}{d_l} = r\left[1 - (r-1)\frac{d_0}{2\sqrt{\pi D_g t}}\right] \tag{9}$$

which is valid, of course, only for $t > r^2 d_0^2/(4\pi D_g)$. The corresponding formula is a little more complicated when the flame is in the outer region,[45] as it may be in 25% oxygen. By focusing on the initial flame transient, however, asymptotic analysis of radiant extinction can always be simplified for sufficiently weak atmospheres.

The droplet-diameter curves in Fig. 6 exhibit a gradual approach to a very small vaporization rate after flame extinction. This small rate is to be expected for quasisteady heptane droplet vaporization in the atmosphere at ambient temperature. Even for these early extinctions, appreciable periods (4 or 5 s) of quasisteady droplet regression are observed during combustion. These periods are sufficient for the initial ignition energy input to become inconsequential. Weaker ambient mixtures would be needed for loss of the inner quasisteady region and fully transient behavior strongly dependent on initial conditions to occur.

In contrast to Figs. 4 and 5, no systematic curvature of droplet-diameter lines is found in Fig. 6, a difference that deserves explanation. As described earlier for the larger droplet of Fig. 5, for all three droplets of Fig. 6 extinction was observed to result in a brief contraction of the soot-particle cloud, followed by a gradual weak and diminishing expansion, eventually leaving stationary soot particles in the vicinity of the stationary droplet, attesting to the extremely low level of ambient gas motion.

Additional Comments on Soot Observations

As indicated earlier, droplets studied here exhibited a certain degree of sooting, the level increasing with increasing oxygen concentration. In the back-lit view of the droplet, visible soot first appears at the moment of ignition. Two lobes of soot clouds stretching from the igniter hoops almost to the droplet surface formed initially on each side of the droplet. These lobes, which developed during the short premixed ignition period, persisted for a brief portion of the droplet lifetime before dispersing into a spherical soot shell during the subsequent diffusion-flame burning. This behavior resembles somewhat that of similar previous drop-tower experiments.[32] Figure 3 shows the structure of the soot shell at different times for the 4-mm droplet burning in the environment of 35% oxygen. Initially, when the diffusion flame lies close to the droplet surface, a thick, almost continuous shell of soot surrounds the droplet, but this almost continuous structure quickly breaks up into well-ordered speckles of soot aggregates, which still surround the droplet at a discrete distance from its surface. Later on, once the droplet diameter shrinks below a certain value, soot production in the region between the droplet surface and the flame ceases. The soot that was formed earlier then aggregates into large clusters, which are carried away by their consequent increased drag.

Soot-shell diameters d_s were measured for all runs by the procedure described earlier. The ratio d_s/d_l was always found to increase with time, except possibly late in the burning history, when soot-cloud diameters are difficult to measure. This increase in d_s/d_l was found to occur in drop-tower studies for smaller droplets[23] and was attributed to the balance between thermophoretic and drag forces. Other previous work[22] showed the ratio d_s/d_l for heptane droplets 0.6–0.9 mm in diameter, burning in air, to correlate with the scaled time t/d_0^2. For this reason, the same scaling was tested for the present data, as shown in Fig. 8. A reasonable correlation is seen to occur in Fig. 8 for all runs except that of the smallest (2-mm) droplet. The 2-mm data lie close to the correlation found previously,[22] whereas the soot standoff ratio d_s/d_l depends more strongly on t/d_0^2 for the larger droplets. Because many different phenomena (such as soot production, growth, and agglomeration) contribute to the results shown in Fig. 8, perfect correlation with t/d_0^2 (which is proportional to t/t_b) is not to be expected. If d_s/d_l marks a balance between drag and thermophoretic forces, then an increase in this ratio with t/d_0^2 would be consistent with an increase in average soot-particle diameter; because of the many uncertainties involved, however, quantitative estimates were not made.

Additional Comments on Burning-Rate Constants

The burning-rate constants K reported in Table 1, averaged between about 1 or 2 s and 3–8 s after ignition, depending on the run, exhibit some interesting systematic variations. They clearly increase with increasing oxygen content of the atmosphere, as is to be expected, and they have the expected general order of magnitude, between 0.9 and 1.4 mm^2/s. In contrast, the value in air is between 0.5 and 0.8 mm^2/s because of the lower diffusivity of nitrogen in comparison with helium. The burning-rate constants show, however, a decrease with increasing initial droplet diameter d_0 in 35% oxygen, no dependence on d_0 in 30% oxygen, and an increase with increasing d_0 in 25% oxygen. These results can be compared with previously published results for heptane droplets having d_0 between 0.2 and 1.8 mm, burning in air. Depending on the experiment, the earlier studies indicate that K increases[18] with d_0, decreases[22] with d_0, or is independent[25] of d_0. Reasoning has been put forward for a decrease as a consequence of increasing contaminant absorption associated with soot formation,[22] and this is consistent with our observed dependence in 35% oxygen, our most highly sooting environment. This argument cannot, however, explain our results in 25% oxygen or those reported by Hara and Kumagai.[18,25] It appears that closer attention may have to be paid to the relative velocity of droplet and gas to explain the results completely. In this work, use may be made of previous results, such as theoretical studies of convective effects on droplet combustion at low Reynolds numbers,[54] as well as correlations for higher Reynolds numbers.[55] Although the convective effects to be explained here are not large, typically less than 20%, more study of their sources is desirable. The additional data to be obtained from the MSL-1 reflight may help to resolve the situation.

Conclusions

The results of the DCE aboard STS-83 provided a great deal of information even though the shortened flight permitted only eight successful runs to be completed. It was established that, at 1 atm and about 300 K ambient temperature in oxygen–helium atmospheres, heptane droplet combustion experiences diffusive extinction for 35% oxygen and radiative extinction for 25% oxygen for droplets of initial diameters between about 2 and 4 mm. At 30% oxygen, diffusive extinction occurs for small droplets (less than about 3-mm initial diameter) and radiative extinction for large droplets (greater than about 4-mm initial diameter). After ignition, the square of the droplet diameter decreases linearly with time even though the flame diameter behaves in a more complex manner that is consistent with current understanding of the dynamics of droplet combustion.

Burning-rate constants increase with increasing oxygen content of the atmosphere and exhibit some variations with initial droplet diameter and with droplet motion. Soot production experiences a rich variety of evolutionary behavior and is much stronger in 35% oxygen than in 25% oxygen. Soot-cloud diameters divided by droplet diameters increase somewhat with time and correlate approximately with time from ignition scaled by the burning time for different initial diameters. Many additional details of the droplet-combustion process were observed and explained.

Much more research remains to be done on the basis of these results. Radiative extinctions need to be analyzed in a quantitative manner theoretically, as do diffusive extinctions for situations in which the flame is influenced by the outer transient zone surrounding the quasisteady burning region. Fuel pyrolysis in the gas and absorption of pyrolysis products by the liquid need to be treated better quantitatively. Many aspects of soot production and soot-particle histories require further attention. As with many fundamental scientific investigations, the present work, thus, has uncovered an appreciable number of additional areas worthy of further study.

Acknowledgments

This research was sponsored by the NASA Microgravity Combustion Science program. We extend sincere thanks to the Microgravity Science Laboratory (MSL-1) crew members, in particular, to Roger Crouch, Gregory Linteris, and Janice Voss for conducting the experiments. We also thank the many individuals at the Payload Operation Control Center at NASA Marshall Space Flight Center in Huntsville, Alabama, for their support and help throughout the mission. Without the dedicated efforts of the engineering team at the NASA Lewis Research Center this flight experiment would not have been possible. Malissa Ackerman helped with the data analysis. The last author thanks D. E. Rosner for discussion of his method on the inference of temperature gradients from thermopherotic effects.

References

[1]Kumagai, S., "Combustion of Fuel Droplets in a Falling Chamber with Special Reference to the Effects of Natural Convection," *Jet Propulsion*, Vol. 26, No. 9, 1956, pp. 786–790.

[2]Kumagai, S., and Isoda, H., "Combustion of Fuel Droplets in a Falling Chamber," *Sixth Symposium (International) on Combustion*, Combustion Inst., Pittsburgh, PA, 1957, pp. 726–731.

[3]Isoda, H., and Kumagai, S., "New Aspects of Droplet Combustion," *Seventh Symposium (International) on Combustion*, Combustion Inst., Pittsburgh, PA, 1959, pp. 523–531.

[4]Faeth, G. M., Dominics, D. P., Tulpinsky, J. F., and Olson, D. R., "Supercritical Bipropellant Droplet Combustion," *Twelfth Symposium (International) on Combustion*, Combustion Inst., Pittsburgh, PA, 1969, pp. 9–18.

[5]Kumagai, S., Sakai, T., and Okajima, S., "Combustion of Free Fuel Droplets in a Freely Falling Chamber," *Thirteenth Symposium (International) on Combustion*, Combustion Inst., Pittsburgh, PA, 1971, pp. 779–785.

[6]Okajima, S., and Kumagai, S., "Further Investigations of Combustion of Free Droplets in a Freely Falling Chamber Including Moving Droplets," *Fifteenth Symposium (International) on Combustion*, Combustion Inst., Pittsburgh, PA, 1975, pp. 401–407.

[7]Knight, B., and Williams, F. A., "Observations on the Burning of Droplets in the Absence of Buoyancy," *Combustion and Flame*, Vol. 38, No. 2, 1980, pp. 111–119.

[8]Williams, F. A., "Droplet Burning," *Combustion Experiments in a Zero-Gravity Laboratory*, edited by T. H. Cohran, Vol. 73, Progress in Astronautics and Aeronautics, AIAA, New York, 1981, pp. 31–61.

[9]Okajima, S., and Kumagai, S., "Experimental Studies on Combustion of Fuel Droplets in Flowing Air Under Zero and High-Gravity Conditions," *Nineteenth Symposium (International) on Combustion*, Combustion Inst., Pittsburgh, PA, 1982, pp. 1021–1027.

[10]Shaw, B. D., Dryer, F. L., and Williams, F. A., "Sooting and Disruption in Spherically Symmetrical Combustion of Decane Droplets in Air," *Acta Astronautica*, Vol. 17, No. 11/12, 1988, pp. 1195–1202.

[11]Avedision, C. T., Yang, J. C., and Wang, C. H., "On Low Gravity Droplet Combustion," *Proceedings of the Royal Society of London*, Vol. A420, 1988, pp. 183–200.

[12]Gokalp, I., Chauveau, C., Richard, J. R., Kramer, M., and Leuckel, W., "Observations on the Low Temperature Vaporization and Envelope or Wake Flame Burning of *n*-Heptane Droplets at Reduced Gravity During Parabolic Flights," *Twenty-Second Symposium (International) on Combustion*, Combustion Inst., Pittsburgh, PA, 1989, pp. 2027–2035.

[13]Yang, J. C., and Avedisian, C. T., "The Combustion of Unsupported Heptane/Hexadecane Mixture Droplets at Low Gravity," *Twenty-Second Symposium (International) on Combustion*, Combustion Inst., Pittsburgh, PA, 1989, pp. 2037–2044.

[14]Chauveau, C., and Gökalp, L., "Experiments on the Burning of *n*-Heptane Droplets in Reduced Gravity," *Proceedings of the Seventh European Symposium on Material Science and Fluid Physics in Microgravity*, Vol. 295, ESA Special Publications, European Space Agency, Paris, 1989, pp. 467–472.

[15]Sato, J., Tsue, M., Niwa, M., and Kono, M., "Effects of Natural Convection on High-Pressure Droplet Combustion," *Combustion and Flame*, Vol. 82, No. 2, 1990, pp. 142–150.

[16]Jackson, G. S., Avedisian, C. T., and Yang, J. C., "Soot Formation During Combustion of Unsupported Methanol/Toluence Mixture Droplets in Microgravity," *Proceedings of the Royal Society of London*, Vol. A435, 1991, pp. 359–369.

[17]Choi, M. Y., Dryer, F. L., and Haggard, J. B., Jr., "Observations on a Slow Burning Regime for Hydrocarbon Droplets, *n*-Heptane/Air Results," *Twenty-Third Symposium (International) on Combustion*, Combustion Inst., Pittsburgh, PA, 1991, pp. 1597–1604.

[18]Hara, H., and Kumagai, S., "Experimental Investigation of Free Droplet Combustion Under Microgravity," *Twenty-Third Symposium (International) on Combustion*, Combustion Inst., Pittsburgh, PA, 1991, pp. 1605–1611.

[19]Cho, S. Y., Choi, M. Y., and Dryer, F. L., "Extinction of a Free Methanol Droplet in Microgravity," *Twenty-Third Symposium (International) on Combustion*, Combustion Inst., Pittsburgh, PA, 1991, pp. 1611–1617.

[20]Yang, J. C., Jackson, G. S., and Avedisian, C. T., "Combustion of Unsupported Methanol/Dodecanol Mixture Droplet at Low Gravity," *Twenty-Third Symposium (International) on Combustion*, Combustion Inst., Pittsburgh, PA, 1991, pp. 1619–1625.

[21]Jackson, G. S., Avedisian, C. T., and Yang, J. C., "Observations of Soot During Droplet Combustion at Low Gravity: Heptane and Heptane/Monochloro–Alkane Mixtures," *International Journal of Heat and Mass Transfer*, Vol. 35, No. 8, 1992, pp. 2017–2033.

[22]Jackson, G. S., and Avedisian, C. T., "Experiments on the Effects of Initial Diameter in Spherically Symmetric Droplet Combustion of Sooting Fuels," AIAA Paper 93-0130, Jan. 1993.

[23]Choi, M. Y., Dryer, F. L., Green, G. J., and Sangiovanni, J. J., "Soot Agglomeration in Isolated, Free Droplet Combustion," AIAA Paper 93-0823, Jan. 1993.

[24]Mikami, M., Kono, M., Sato, J., Dietrich, D. L., and Williams, F. A., "Combustion of Miscible Binary-Fuel Droplets at High Pressure Under Microgravity," *Combustion Science and Technology*, Vol. 90, Nos. 1–4, 1993, pp. 111–123.

[25]Hara, H., and Kumagai, S., "The Effect of Initial Diameter on Free Droplet Combustion with Spherical Flame," *Twenty-Fifth Symposium (International) on Combustion*, Combustion Inst., Pittsburgh, PA, 1994, pp. 423–430.

[26]Mikami, M., Kato, H., Sato, J., and Kono, M., "Interactive Combustion of Two Droplets in Microgravity," *Twenty-Fifth Symposium (International) on Combustion*, Combustion Inst., Pittsburgh, PA, 1994, pp. 431–438.

[27]Mikami, M., Niwa, M., Kato, H., Sato, J., and Kono, M., "Clarification of the Flame Structure of Droplet Burning Based on Temperature Measurement in Microgravity," *Twenty-Fifth Symposium (International) on Combustion*, Combustion Inst., Pittsburgh, PA, 1994, pp. 439–446.

[28]Tanabe, M., Kono, M., Sato, J., Koenig, J., Eigenbrod, C., and Rath, H., "Effects of Natural Convection on Two Stage Ignition of a *n*-Dodecane Droplet," *Twenty-Fifth Symposium (International) on Combustion*, Combustion Inst., Pittsburgh, PA, pp. 455–461.

[29]Chauveau, C., Chesneau, X., and Gökalp, I., "High Pressure Vaporization and Burning of Methanol Droplets in Reduced Gravity," *Advances in Space Research*, Vol. 16, No. 7, 1995, pp. 157–160.

[30]Marchese, A. J., Dryer, F. L., Colantonio, R. O., and Nayagam, V., "Microgravity Combustion of Methanol and Methanol/Water Droplets: Drop Tower Experiments and Model Predictions," *Twenty-Sixth Symposium (International) on Combustion*, Combustion Inst., Pittsburgh, PA, 1996, pp. 1209–1217.

[31]Marchese, A. J., Dryer, F. L., Nayagam, V., and Colantonio, R. O., "Hydroxyl Radical Chemiluminescence Imaging and the Structure of Microgravity Droplet Flames," *Twenty-Sixth Symposium (International) on Combustion*, Combustion Inst., Pittsburgh, PA, 1996, pp. 1219–1226.

[32]Choi, M. Y., and Lee, K. O., "Investigation of Sooting in Microgravity Droplet Combustion," *Twenty-Sixth Symposium (International) on Combustion*, Combustion Inst., Pittsburgh, PA, 1996, pp. 1243–1249.

[33]Tsue, M., Segawa, D., Kadota, T., and Yamasaki, H., "Observation of Sooting Behavior in an Emulsion Droplet Flame by Planar Laser Light Scattering in Microgravity," *Twenty-Sixth Symposium (International) on Combustion*, Combustion Inst., Pittsburgh, PA, 1996, pp. 1251–1258.

[34]Vieille, B., Chauvenau, C., Chesneau, X., Odeide, A., and Gökalp, I., "High-Pressure Droplet Burning Experiments in Microgravity," *Twenty-Sixth Symposium (International) on Combustion*, Combustion Inst., Pittsburgh, PA, 1996, pp. 1259–1265.

[35]Dietrich, D. L., Haggard, J. B., Jr., Dryer, F. L., Nayagam, V., Shaw, B. D., and Williams, F. A., "Droplet Combustion Experiments in Spacelab," *Twenty-Sixth Symposium (International) on Combustion*, Combustion Inst., Pittsburgh, PA, 1996, pp. 1201–1207.

[36]Card, J. M., and Williams, F. A., "Asymptotic Analysis of the Structure and Extinction of Spherically Symmetrical *n*-Heptane Diffusion Flame," *Combustion Science and Technology*, Vol. 84, No. 1–6, 1992, pp. 91–119.

[37]Card, J. M., and Williams, F. A., "Asymptotic Analysis with Reduced Chemistry for the Burning of *n*-Heptane Droplet," *Combustion and Flame*, Vol. 91, No. 2, 1992, pp. 187–199.

[38]Card, J. M., "Asymptotic Analysis for the Burning of *n*-Heptane Droplets Using a Four-Step Reduced Mechanism," *Combustion and Flame*, Vol. 93, No. 4, 1993, pp. 375–390.

[39]Lindstedt, R. P., and Maurice, L. Q., "Detailed Kinetic Modelling of *n*-Heptane Combustion," *Combustion Science and Technology*, Vol. 107, Nos. 4–6, 1995, pp. 317–353.

[40]Bollig, M., Pitsch, H., Hewson, J. C., and Seshadri, K., "Reduced *n*-Heptane Mechanism for Non-Premixed Combustion with Emphasis on Pollutant-Relevant Intermediate Species," *Twenty-Sixth Symposium (International) on Combustion*, Combustion Inst., Pittsburgh, PA, 1996, pp. 729–737.

[41]Seshadri, K., Bollig, M., and Peters, N., "Numerical and Asymptotic Studies of the Structure of Stoichiometric and Lean Premixed Heptane Flames," *Combustion and Flame*, Vol. 108, No. 4, 1997, pp. 518–536.

[42]Held, T. J., Marchese, A. J., and Dryer, F. L., "A Semi-Empirical Reaction Mechanism for *n*-Heptane Oxidation and Pyrolysis," *Combustion Science and Technology*, Vol. 123, Nos. 1–6, 1997, pp. 107–146.

[43]Klimek, R. B., Wright, T. W., and Sielken, R. S., "Color Image Processing and Object Tracking System," NASA TM-107144, Feb. 1996.

[44]Shaw, B. D., Dryer, F. L., and Williams, F. A., "Interactions Between Gaseous Electrical Discharges and Single Liquid Droplets," *Combustion and Flame*, Vol. 74, No. 3, 1988, pp. 233–254.

[45]Crespo, A., and Liñán, A., "Unsteady Effects in Droplet Evaporation and Combustion," *Combustion Science and Technology*, Vol. 11, No. 1, 1975, pp. 9–18.

[46]Fachini, F. F., and Liñán, A., "Transient Effects in Droplet Ignition Phenomenon," *Combustion and Flame*, Vol. 109, No. 3, 1997, pp. 303–313.

[47]King, M. K., "An Unsteady-State Analysis of Porous Sphere and Droplet Fuel Combustion Under Microgravity Conditions," *Twenty-Seventh Symposium (International) on Combustion*, Combustion Inst., Pittsburgh, PA, 1997, pp. 1227–1234.

[48]Chao, B. H., Law, C. K., and T'ien, J. S., "Structure and Extinction of Diffusion Flames with Flame Radiation," *Twenty-Third Symposium (International) on Combustion*, Combustion Inst., Pittsburgh, PA, 1990, pp. 523–531.

[49]Ubhayakar, S. K., and Williams, F. A., "Burning and Extinction of a Laser-Ignited Carbon Particle in Quiescent Mixtures of Oxygen and Nitrogen," *Journal of the Electrochemical Society*, Vol. 123, No. 5, 1976, pp. 747–756.

[50]Sohrab, S. H., Liñán, A., and Williams, F. A., "Asymptotic Theory of Diffusion-Flame Extinction with Radiant Loss from the Flame Zone," *Combustion Science and Technology*, Vol. 27, Nos. 3, 4, 1982, pp. 143–154.

[51]Marchese, A. J., and Dryer, F. L., "The Effect of Non-Luminous Thermal Radiation in Microgravity Droplet Combustion," *Combustion Science and Technology*, Vol. 124, Nos. 1–6, 1997, pp. 371–402.

[52]Rightley, M. L., and Williams, F. A., "Structures of CO Diffusion Flames Near Extinction," *Combustion Science and Technology*, Vol. 125, Nos. 1–6, 1997, pp. 181–200.

[53]Buckmaster, J., Stewart, D. S., Ignatiadis, A., and Williams, M., "On the Wind Generated by a Collapsing Diffusion Flame," *Combustion Science and Technology*, Vol. 46, Nos. 3–6, 1980, pp. 145–165.

[54]Gogos, G., Sadhal, S. S., Ayyaswamy, P. S., and Sundararajan, T., "Thin-Flame Theory for the Combustion of a Moving Liquid Drop: Effects Due to Variable Density," *Journal of Fluid Mechanics*, Vol. 171, 1986, pp. 121–144.

[55]Law, C. K., and Williams, F. A., "Kinetics and Convection in the Combustion of Alkane Droplets," *Combustion and Flame*, Vol. 19, 1972, pp. 393–405.

G. M. Faeth
Editor-in-Chief